JOURNAL OF PROPULSION AND POWER
Vol. 22, No. 4, July–August 2006

Burning of Ammonium–Perchlorate Ellipses and Spheroids in Fuel Binder

X. Wang,* J. Buckmaster,† and T. L. Jackson‡
University of Illinois at Urbana–Champaign, Urbana, Illinois 61801

Our simulations of heterogeneous propellant combustion have always assumed that the oxidizer particles (ammonium perchlorate) are disks (two dimensional) or spheres (three dimensional). Here the effects on the burning rate are examined when the disks/spheres are replaced by ellipses/ellipsoids. In two dimensions, it is shown that an area-preserving deformation of a pack of disks, generating a pack of ellipses, can lead to significant variations in the burning rate. However, if the ellipses are randomly packed, so that the alignment of their axes is random, the shape effect is small. In three dimensions, volume-preserving deformation, which generates ellipsoids, leads to burning rate changes no greater than those in two dimensions. Absent a random packing algorithm for ellipsoids, it is speculated that here also a random alignment of the axes would eliminate the effect.

I. Introduction

RECENT years have seen significant advances in the modeling of heterogeneous propellant combustion, specifically in the context of ammonium–perchlorate (AP)/hydroxyl-terminated-polybutadiene propellants. In Ref. 1, a two-dimensional treatment, a numerical code is described in which the combustion field is fully coupled to heat conduction in the solid via a nonuniformly regressing nonplanar surface. The corresponding three-dimensional problem is described in Refs. 2 and 3, the first using two-step kinetics and the second three-step kinetics. Comparisons between the numerical results and experimental results of Miller[4] show that the effects of propellant morphology on burning rates can be satisfactorily predicted over a wide pressure range. At fixed pressure, the variations in burning rate due to different morphologies are as much as threefold, so that these are nontrivial predictions.

In this connection, note how we chose the values of the numerous parameters for this problem, parameters identified in Refs. 1–3. Most are typical values defined by the community at large. Some are uncertain, of course, particularly the surface pyrolysis parameters, but once a choice was made no post hoc adjustments were made to better fit the three-dimensional data of Miller. An important parameter subset is those of the gas kinetics, the reaction rates for the two-step and three-step kinetics. There, we used one-dimensional burning rate data for pure AP and for homogeneous blends of AP and binder. The use of a three-step mechanism enabled us to fit blend burning rates over a wide range of mixture ratios, and it is presumably for this reason that the three-step results are more accurate than the two-step results. Most important, our calculations are not a massive exercise in curve fitting.

This does not mean that better choices for some of our parameter values are not possible. Although we reasonably capture qualitative aspects of sandwich burning,[3] most notably the surface topography, the surface topography in our three-dimensional simulations does not show concavity in the surfaces of large AP particles at pressures for which it is observed experimentally. It seems probable that this could be rectified by suitable adjustment of the pyrolysis parameters, but we have not yet attempted to do so. The reason for this is that if at any time a parameter is changed the curve fitting of the one-dimensional burning rates must be redone and, overall, this is a time-consuming and expensive proposition. Nevertheless, we believe that the combustion codes (two and three dimensional), with the parameters presently in place, can be used to explore a number of propellant-burning issues. For example, we recently examined the response to small-pressure disturbances created by an impinging acoustic wave.[5]

The results of Ref. 1 are for random packs of AP disks and those of Refs. 2 and 3 for random packs of AP spheres. However, real AP particles are not spherical and so it is appropriate to investigate the consequences of the simplification. We do this here by examining AP particles in the shape of ellipses (two dimensional) or spheroids (three dimensional). Figure 1 shows a scanning electron microscope picture of AP particles of nominal diameter 200 μm, and this gives some sense of the variations in shape that occur in practice.

II. Ellipse Packs

The random packing algorithm that is used to generate disk packs or sphere packs is described in Refs. 6 and 7, and is based on work by Lubachevsky et al.[8] An infinite computational domain is defined by the periodic continuation of a square or cube, and points are randomly assigned to this domain at time $t = 0$ with random velocities. For $t > 0$, the points become disks or spheres that grow linearly with t with a distribution of rates that defines the final distribution of AP diameters. Collisions between the particles are dealt with using straightforward but nonclassical dynamics, and this prevents overlapping. The pack is defined by stopping the calculation at some assigned time, or after the interval between collisions becomes too small to continue.

Packs generated in this fashion can be designed to capture the volume fractions of the various-sized particles in experimental or industrial packs.

Extending the packing algorithm to more complex shapes is a major undertaking because the identification of collision events is then more challenging and particle rotation must be accounted for. The code that we have developed for this purpose can only generate modestly sized two-dimensional packs, but we present some results obtained within that framework. We also, but with no limitation on pack complexity, examine packs generated by the isochoric deformation of a disk pack. In a later section, we examine deformed sphere packs.

A. Isochorically Deformed Disk Packs

To construct a pack of ellipses we can start with a pack of disks and stretch it in the x direction by an amount α and in the y direction

Received 25 January 2005; revision received 14 April 2005; accepted for publication 14 April 2005.

*Scientist, Center for Simulation of Advanced Rockets, 1304 West Springfield Avenue; wang@uiuc.edu.

†Professor, Department of Aerospace Engineering, 104 South Wright Street; limey@uiuc.edu.

‡Senior Scientist, Center for Simulation of Advanced Rockets, 1304 West Springfield Avenue; tlj@csar.uiuc.edu.

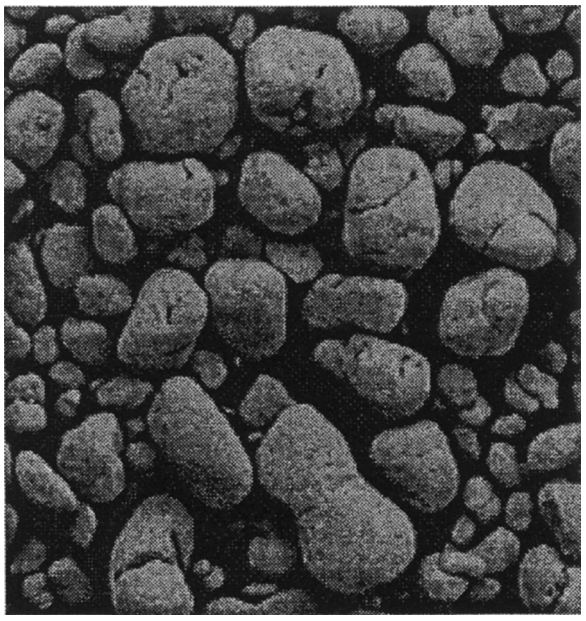

Fig. 1 SEM photograph of AP particle pack, courtesy of H. Krier.

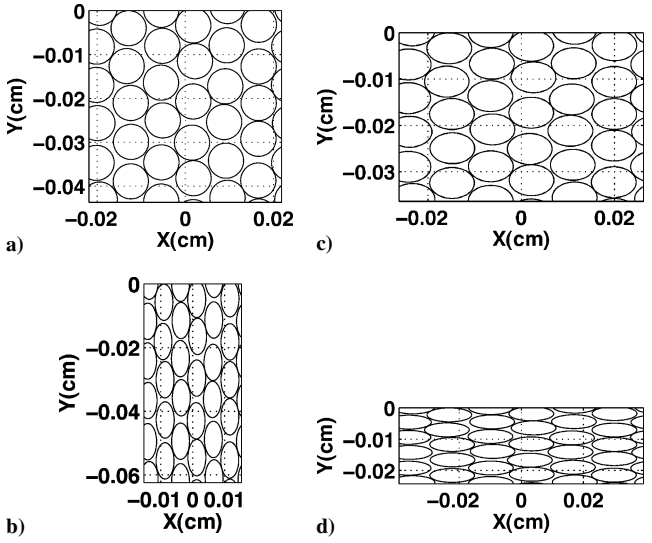

Fig. 2 Elliptic packs generated by isochoric (area-preserving) deformation: *a/b* = a) 1, b) 0.7, c) 1.2, and d) 1.8.

by an amount $1/\alpha$, thus preserving the area. Then the circle

$$x = r\cos\theta, \qquad y = r\sin\theta \tag{1}$$

becomes the ellipse

$$x = \alpha r\cos\theta, \qquad y = (r/\alpha)\sin\ \theta \tag{2}$$

that is,

$$(x/\alpha r)^2 + (\alpha y/r)^2 = 1 \tag{3}$$

with aspect ratio $a/b = \alpha^2$, where a and b are the semi-axes. Figure 2a shows an initial monomodal disk pack (particle diameter 80 μm). It is a square of side 436.7 μm and contains 30 particles with centers in the domain. Figures 2b–2d show ellipse packs generated by deforming this pack using different values of α. The packing fraction (volume fraction of AP) is 0.79. Figure 3a shows a multimodal disk pack (Table 1) from which ellipse packs have been generated, for example, Fig. 3b.

To burn these packs, we use the code described in Ref. 1, here using the Oseen model in the gas phase, rather than the full

Table 1 Data for the multimodal disk pack of Fig. 3a

No. of particles	Diameter, μm	No. fractions[a]	Volume fractions[b]
5	80	0.005	0.12190
10	50	0.01	0.09538
25	40	0.025	0.15247
60	30	0.06	0.20584
450	10	0.45	0.17153
450	5	0.45	0.04288

[a]Number fractions add to 1.
[b]Volume fractions add to 0.79, the overall packing fraction of AP.

Table 2 Parameter values from Ref. 1

Parameter	Value
D_1[a]	33.862 gm/cm$^3 \cdot$ s $\cdot$ bar^{n1}
D_2[a]	894822.5 gm/cm$^3 \cdot$ s $\cdot$ bar^{n2}
E_1/R_u[a]	2,500 K
E_2/R_u[a]	9,000 K
n_1[a]	2.0876
n_2[a]	0.4531
Q_{g1}[a]	480 kcal/kg
Q_{g2}[a]	4,703 kcal/kg
$A_{\rm AP}$[b]	43,973 cm/s
A_B[b]	1035.95 cm/s
$E_{\rm AP}/R_u$[b]	10,000 K
E_B/R_u[b]	7,500 K
$Q_{\rm AP}$[b]	-150 kcal/kg
Q_B[b]	-66 kcal/kg
β[c]	7.936
$\rho_{\rm AP}$[d]	1,950 kg/m^3
ρ_B[d]	920 kg/m^3
$\lambda_{\rm AP}$[e]	0.405 W/m $\cdot$ K
λ_B[e]	0.276 W/m $\cdot$ K

[a]Parameters for two-step kinetics.
[b]Parameters for the pyrolyis laws.
[c]Mass ratio of AP to binder at stoichiometry.
[d]Solid density.
[e]Solid conductivity.

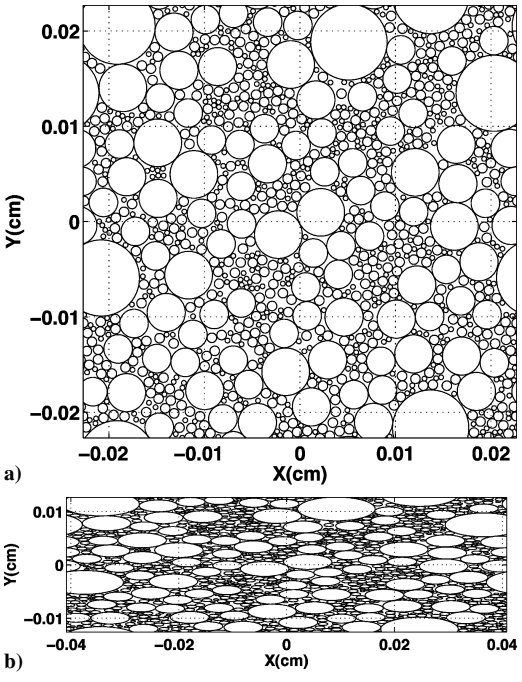

Fig. 3 Multimodal disk pack, $N = 1000$: a) *a/b* = 1, domain size 453.92 μm and b) *a/b* = 1.8.

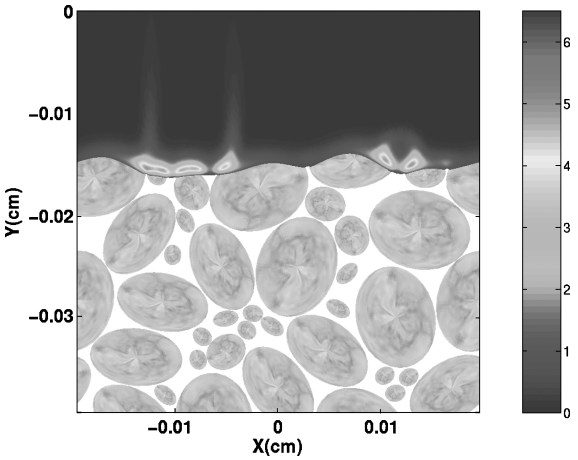

Fig. 4 Instantaneous combustion field for random pack of ellipses, $p = 20$ atm.

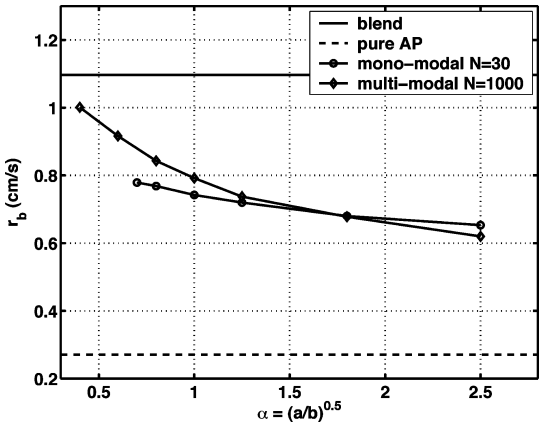

Fig. 5 Burning rates vs α for the Figs. 2 and 3 packs, 20 atm.

Navier–Stokes equations. (Parameters are shown in Table 2 and discussed in Ref. 1.) This simplification, a useful one, is discussed in Ref. 2 and is quite accurate in determining mean burning rates. Figure 4 shows the instantaneous combustion field and propellant surface profile for one of the packs that we discuss in this paper and hints at the complexity of the combustion code. In Fig. 4, the contours are measures of the total heat output from chemical reaction. The strong structures are diffusion flames, and over the AP particles sit weak decomposition flames. The gas-phase combustion field shown here is coupled to unsteady heat conduction in the solid via the nonuniformly, nonsteadily retreating interface, and the average speed of this retreat defines the burning rate.

Thus, Fig. 5 is constructed and shows variations of the mean burning rate with α for various packs of the type shown in Figs. 2 and 3. The pressure is 20 atm. Also shown in Fig. 5 is the burning rate for a stoichiometric blend of fine AP and binder (1.081 cm/s) and that for pure AP (0.265 cm/s).

The trends are clear and not surprising. For small values of a/b, a region of AP on the surface is always close to a region of binder, increasing the degree of reactant mixing that occurs during the passage from the surface through the flame field and, thus, driving the burning rate closer to the blend value. For large values of a/b, the surface is characterized by large segments of AP, thus, driving the burn rate closer to the pure AP values. For small values of a/b, the surface resembles that defined by small circular disks; for large values, it resembles that defined by large circular disks. Burning trends with AP size have long been understood and are captured by the simulations of Refs. 2 and 3. For fixed propellant morphology, high pressures (particles large compared to the flame thickness) lead to burning rates that approach those of pure AP; low pressures (particles small compared to the flame thickness) lead to burning rates that approach those of the blend. From Fig. 5 we see that the effects of noncircularity are strongest for the multimodal pack when $a/b < 1$.

B. Monomodal Random Ellipse Packs

As we noted earlier, packing ellipses is harder than packing disks. For example, the time from one collision to the next is the minimum of the collision times calculated for all pairs of particles. For disks, a quadratic equation is solved to determine the latter; for ellipses, a quartic is solved. (Then Ref. 9 is of value.) Overall, the methods are similar to those of Ref. 10.

For comparison with the results for the packs of Fig. 2, we have constructed packs with number of particles $N = 30$, a computational domain identical to that of Fig. 2a, that is, a square of side 436.7 μm, and identical particle area so that

$$\pi ab = \pi D^2/4 \tag{4}$$

where $D = 80$ μm. Figure 6 shows four different packs for different values of a/b, and Fig. 7 shows the corresponding burning rates.

When these results for 20 atm are compared with those of Fig. 5, note that for the latter a/b can vary from zero to infinity because both the aspect ratio and the alignment are prescribed, but for the former only the aspect ratio (>=1) is prescribed because, in

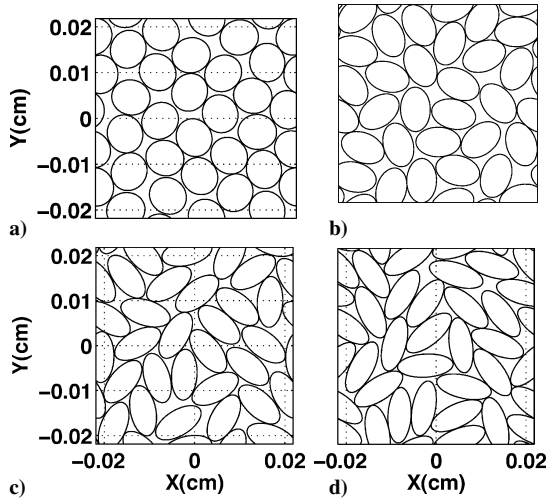

Fig. 6 Random packs: $N = 30$, equivalent disk diameter 80 μm, domain size 436.7 μm, packing fraction 0.79, and aspect ratios a) 1.1, b) 1.5, c) 2, and d) 2.4.

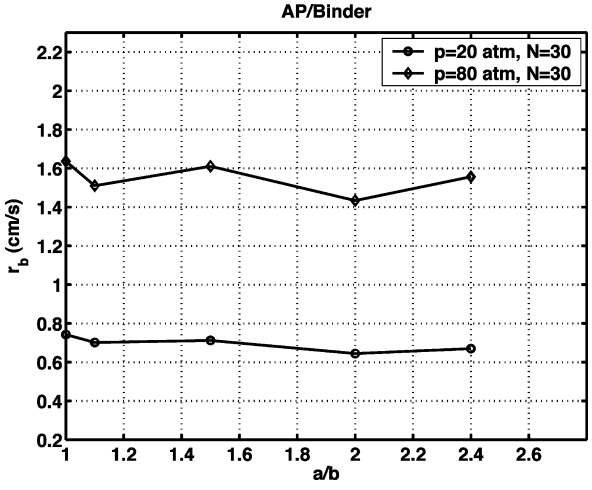

Fig. 7 Burning rates for monomodal random packs of Fig. 6, at 20 and 80 atm.

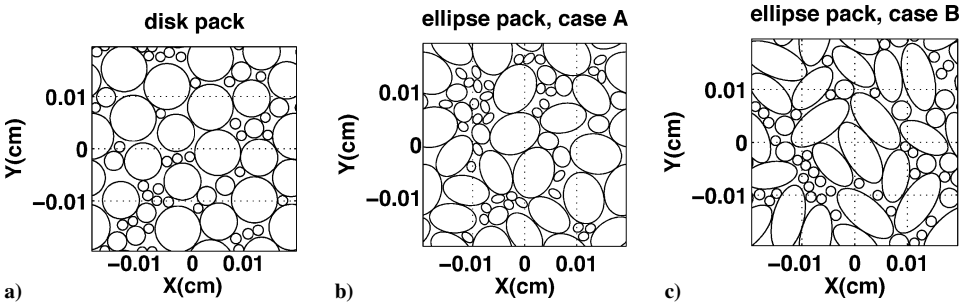

Fig. 8 Multimodal random packs, $N = 66$, and packing fraction 0.79: a) disks, b) ellipses, case A, and c) ellipses, case B.

Table 3 Data for the packs of Fig. 8, disks, case A, and case B

		$2a/2b$	
Number	Disk diameter, μm	Case A	Case B
10	87.7	100/76.9	130.1/59.1
10	71.2	90/56.3	100.6/50.3
10	36.5	40/33.3	44.7/29.8
16	19.8	25/15.6	25.8/15.2
20	18.3	20/16.7	22.4/14.9

principle, there is no difference between, for example, $a/b = 1.5$ and $a/b = 1/1.5 = 0.67$.

In contrast to the results for the deformed pack of Fig. 5, the random pack results (Fig. 7) show no discernable trends in burning rate with a/b. There are variations, more noticeable for $p = 80$ atm than for $p = 20$ atm, but these are of the same order of magnitude as those that arise when different seeds are used to generate otherwise identical packs, or when the packs of Fig. 6 are burnt from the sides or from bottom to top: These packs are not statistically homogeneous. Comparable variations arise for packs with $N = 100$, $D = 50$ μm, and we are unable to create packs large enough to make these variations negligable, but our interpretation of these results is that when the particle alignment is random the effects of aspect ratio are small. The results of the next section support this view.

C. Multimodal Random Ellipse Packs

We noted in the preceding section that for monomodal packs with $N = 30$ or $N = 100$, variations in the burning rate reflect the fact that packs of this small size are not statistically homogeneous. Because, at this time, we are unable to construct much larger packs, we can only deal with this difficulty by burning a large number of packs and averaging. The different packs are generated by using different seeds, or by rotation. We use this strategy here for multimodal random packs, $N = 66$. Figure 8 shows samples of three different pack types, the data for which are given in Table 3. The particle areas are fixed across each row.

Figure 9 shows averaged burning rates for the three cases at different pressures, and although there is a trend, it is small. The rates for the four increasing pressures are 0.6745, 0.700, and 0.713; 1.0345, 1.057, and 1.09; 1.30, 1.3334, and 1.401; and 1.5757, 1.624, and 1.634 cm/s. (A sample combustion field for case A is shown in Fig. 4.) Thus, we conclude that there is no significant effect of shape on burning rates if the particle alignments are random.

III. Burning of Spheroid Packs

Our focus so far has been on the two-dimensional problem for two reasons. First, the computational requirements of the three-dimensional combustion problem are large, and this makes parameter exploration difficult. Second, to achieve the desired packing fraction of AP in three dimensions requires a multimodal pack with a large number of particles, and at the present time, we do not have the ability to generate such packs for nonspherical particles. What we can do is generate a multimodal pack of spheres and deform it isochorically, however, and in this section we present some results of this kind.

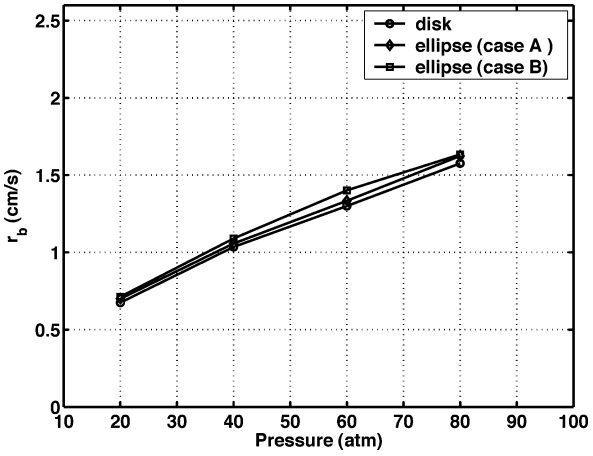

Fig. 9 Averaged burning rates for the multimodal random packs of Fig. 8.

Table 4 Data for sphere pack of Fig. 10

Number	Diameter, μm
1	126.50
2	87.75
1	77.35
2	70.93
2	65.04
3	59.64
3	54.69
4	50.15
5	45.99
6	42.17
7	38.67
9	35.46
11	32.52
14	29.82
17	27.34
21	25.07
26	22.99
32	21.08
40	19.33
53	17.73
66	16.26
83	14.91
104	13.67
130	12.54
162	11.50
199	10.54

We consider a pack of 1003 spheres of packing fraction 0.761 and the size distribution defined by Table 4. Slices through the pack are shown in Fig. 10. This pack is deformed isochorically by stretching it by a factor $\sqrt{\alpha}$ in the x and y directions and by a factor $1/\alpha$ in the z direction so that the sphere

$$x = R\sin\phi\cos\theta, \qquad y = R\sin\phi\sin\theta, \qquad z = R\cos\phi \quad (5)$$

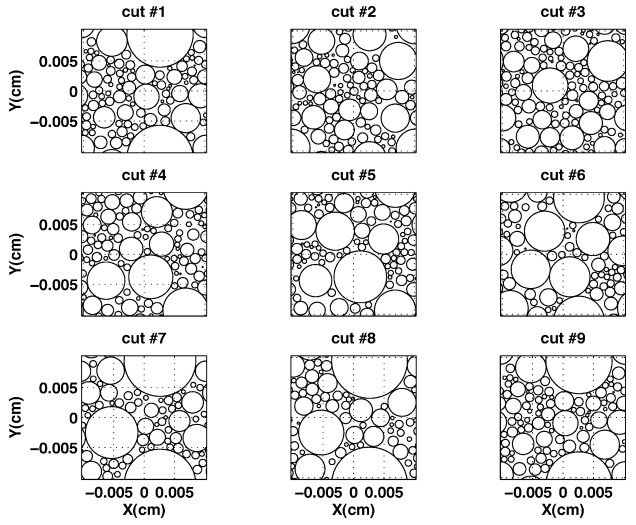

Fig. 10 Slices through pack defined by Table 4, packing fraction 0.761.

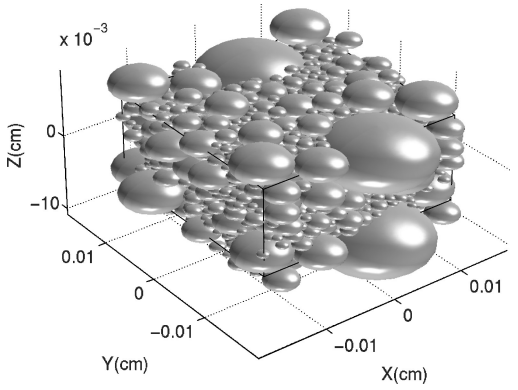

Fig. 11 Deformed form of pack of Fig. 10, $\alpha = 1.8$.

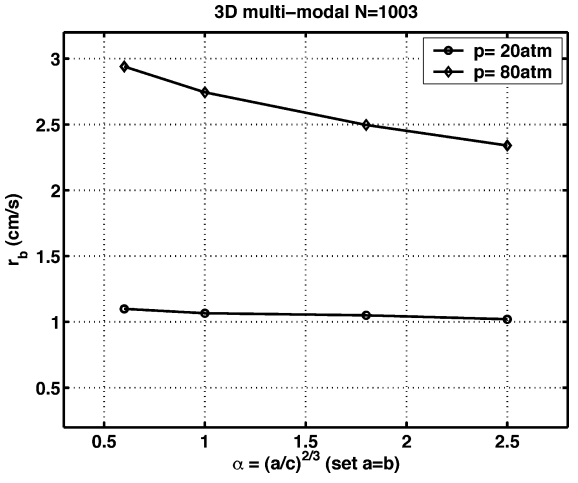

Fig. 12 Burning rates for isochorically deformed three-dimensional packs.

becomes the ellipsoid

$$x = \sqrt{\alpha} R \sin\phi \cos\theta, \qquad y = \sqrt{\alpha} R \sin\phi \sin\theta$$
$$z = (1/\alpha) R \cos\phi \tag{6}$$

with the equation

$$\left(x/\sqrt{\alpha}R\right)^2 + \left(y/\sqrt{\alpha}R\right)^2 + (\alpha z/R)^2 = 1 \tag{7}$$

Figure 11 shows the deformed pack when $\alpha = 1.8$, and burning rates are shown in Fig. 12. The effects of deformation are comparable to those seen in the two-dimensional calculations, and so we believe that here also the effects would be small if the particle orientation were random.

IV. Conclusions

We have examined the burning rate of ellipses and ellipsoids to see if these differ in any significant fashion from those of disks and spheres. The preponderance of evidence shows that they do not. Area-preserving deformations of disks to form ellipses lead to significant changes in burning rate, but if random packs of ellipses with randomly aligned axes are burnt, these changes are not merely reduced, as one would expect, but are eliminated. Aligned spheroids also burn at rates that differ from those of spheres, but these changes are comparable in magnitude to those observed in two dimensions, and so we conjecture that they also would be eliminated if the axes were randomly aligned. Evidence beyond a reasonable doubt would require the construction of random multimodal packs of spheroids, and to construct an algorithm for this purpose would require enormous effort. At this time, our resources are probably better spent elsewhere.

Acknowledgments

This work was supported by the U.S. Department of Energy through the University of California under Subcontract B341494. J. Buckmaster is also supported by the Air Force Office of Scientific Research and by the NASA John H. Glenn Research Center at Lewis Field.

References

[1]Jackson, T. L., and Buckmaster, J., "Heterogeneous Propellant Combustion," *AIAA Journal*, Vol. 40, No. 6, 2002, pp. 1122–1130.

[2]Massa, L., Jackson, T. L., Buckmaster, J., and Campbell, M., "Three-Dimensional Heterogeneous Propellant Combustion," *Proceedings of the Combustion Institute*, Vol. 29, 2002, pp. 2975–2983.

[3]Massa, L., Jackson, T. L., and Buckmaster, J., "New Kinetics for a Model of Heterogeneous Propellant Combustion," *Journal of Propulsion and Power*, Vol. 21, No. 5, 2005, pp. 914–924.

[4]Miller, R. R., "Effects of Particle Size on Reduced Smoke Propellant Ballistics," AIAA Paper 82-1096, June 1982.

[5]Buckmaster, J., Jackson, T. L., Massa, L., and Ulrich, M., "Response of a Burning Heterogeneous Propellant to Small Pressure Disturbances," *Proceedings of the Combustion Institute*, Vol. 30, 2005, pp. 2079–2086.

[6]Knott, G. M., Jackson, T. L., and Buckmaster, J., "The Random Packing of Heterogeneous Propellants," *AIAA Journal*, Vol. 39, No. 4, 2001, pp. 678–686.

[7]Kochevets, S., Buckmaster, J., Jackson, T. L., and Hegab, A., "Random Packs and Their Use in the Modeling of Heterogeneous Solid Propellant Combustion," *Journal of Propulsion and Power*, Vol. 17, No. 4, 2001, pp. 883–891.

[8]Lubachevsky, B. D., Stillinger, F. H., and Pinson, E. N., "Disks vs Spheres: Contrasting Properties of Random Packings," *Journal of Statistical Physics*, Vol. 64, No. 3/4, 1991, pp. 501–524.

[9]Weisstein, E. W., "Quartic Equation," MathWorld—A Wolfram Web Resource, http: mathworld.wolfram.com/QuarticEquation.html [cited 2 May 2005].

[10]Frenkel, D., and Maguire, J. F., "Molecular Dynamics Study of the Dynamical Properties of an Assembly of Infinitely Thin Hard Rods," *Molecular Physics*, Vol. 49, No. 2, 1983, pp. 503–541.